Angewandte Chemie
Eine Zeitschrift der Gesellschaft Deutscher Chemiker

Supporting Information

Silver Makes Better Electrical Contacts to Thiol-Terminated Silanes than Gold

Haixing Li[+], Timothy A. Su[+], María Camarasa-Gómez[+], Daniel Hernangómez-Pérez, Simon E. Henn, Vladislav Pokorný, Caravaggio D. Caniglia, Michael S. Inkpen, Richard Korytár, Michael L. Steigerwald, Colin Nuckolls,* Ferdinand Evers,* and Latha Venkataraman**

ange_201708524_sm_miscellaneous_information.pdf

Table of Contents

I. Additional Figures

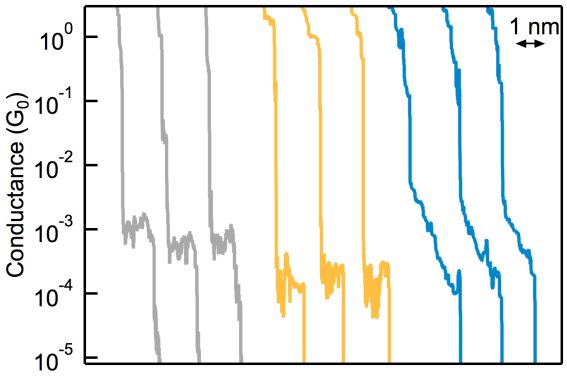

Figure S1. Sample conductance traces of **Si6** measured with Ag (grey), Au (yellow) and Pt (blue) electrical contacts.

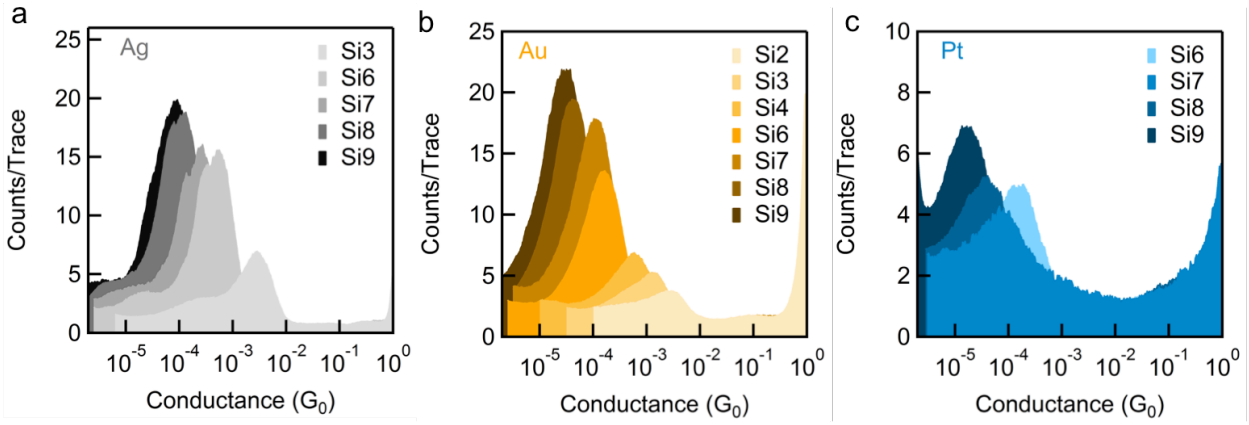

Figure S2. One-dimensional logarithmically-binned conductance histograms for junctions of thiol-terminated (a) **Si3** and **Si6** - **Si9** with Ag electrodes, (b) **Si2** – **Si4** and **Si6** - **Si9** with Au electrodes, (c) **Si6** - **Si9** with Pt electrodes.

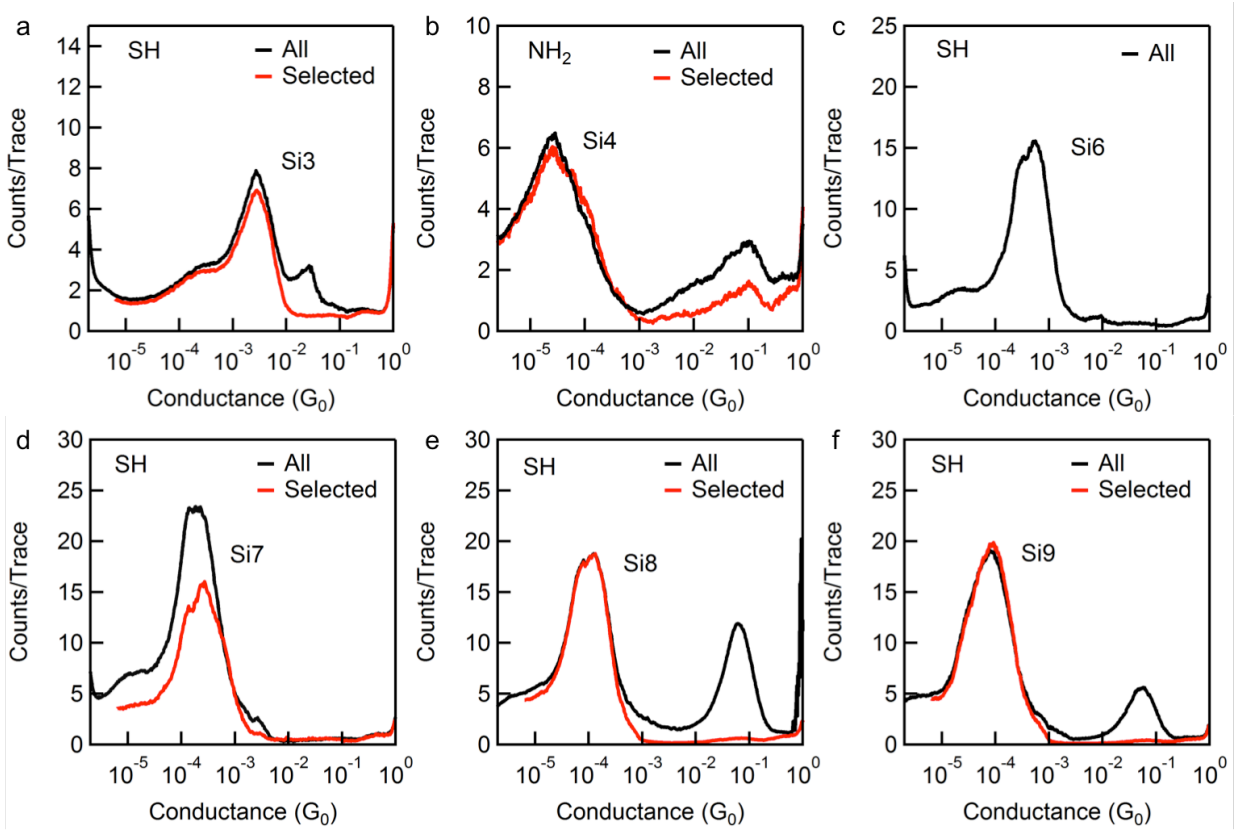

Figure S3. One-dimensional logarithmically-binned conductance histograms compiled from all measured traces (black) and selected traces without oxygen feature (red) for junctions of amine and thiol terminated silanes with Ag electrodes. For thiol-terminated molecules, traces that show significant long features between $0.5G_0$ and 5×10^{-5} G_0 were removed; for amine-terminated molecules, the measured traces that show features longer than 0.2 nm between 0.5 Go and 0.001 Go were removed; both using an automated algorithm. For thiol-terminated **Si6**, histogram (Figure c) of all traces does not show an oxygen peak, thus no selection was applied.

Molecule	Si3-SH	Si6-SH	Si7-SH	Si9-SH	Si4-NH2
# of collected traces	17600	4500	4590	4000	3420
# of selected traces	15181	4500	2904	3316	1074

Table 1. The number of collected traces (top row) and the number of traces selected after applying an automated algorithm (bottom row) are listed for all molecules measured with Ag electrodes.

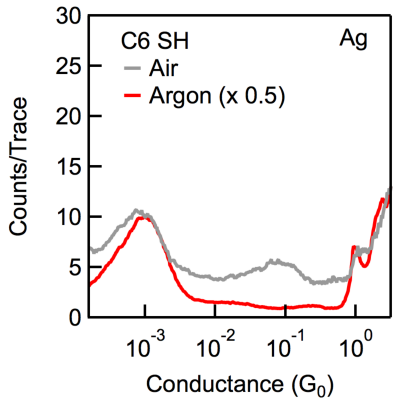

Figure S4. Conductance histograms for measurements of a self-assembled **C6** monolayer on template-stripped Ag prepared with no exposure to oxygen, measured under argon (red). STM-BJ measurements were carried out following methods described in Inkpen et al, Chem. Sci. 2017 in an argon atmosphere.[1] Results from a comparable measurement under ambient conditions (grey) is shown as a comparison. No significant difference in the molecular conductance peak position (around 0.001 G_0) is observed.

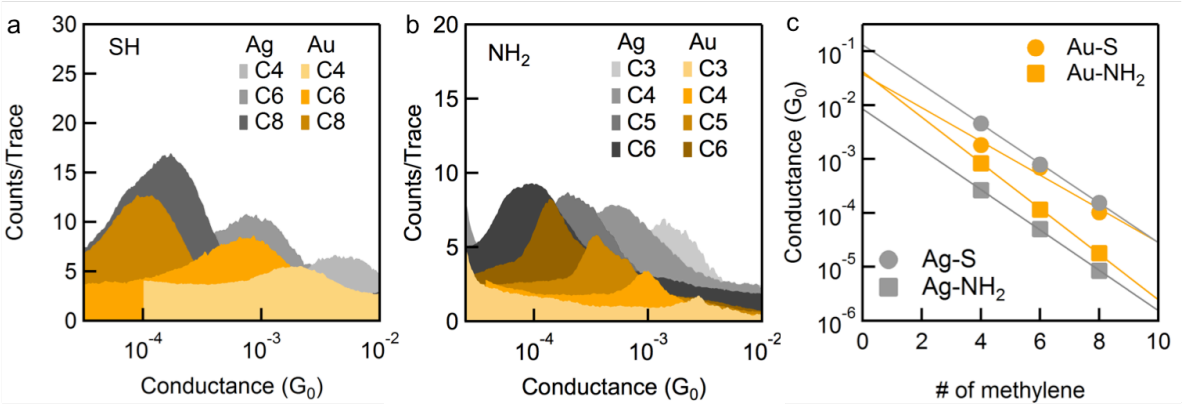

Figure S5. One-dimensional logarithmically-binned conductance histograms for junctions of (a) thiol-terminated **C4, C6** and **C8** and (b) amine-terminated **C3**, **C4, C5** and **C6** with Ag and Au electrodes. Data for the amine-terminated alkanes are reproduced from Kim *et al.*[2] (c) Conductance peak values plotted against the number of methylene in the backbone on a semi-log scale. Square marker: amine-linked junctions; dot marker: thiol-linked junctions. An exponential decrease in conductance with increasing carbon chain length is observed. Lines show linear fits to the data following $G = G_c e^{-\beta n}$ and corresponding decay values are 0.72 ± 0.14 n^{-1} and 0.97 ± 0.01 n^{-1} for Au—S and Au—NH_2 junctions (orange) and 0.85 ± 0.06 n^{-1} and 0.86 ± 0.02 n^{-1} for Ag—S and Ag—NH_2 junctions (grey).

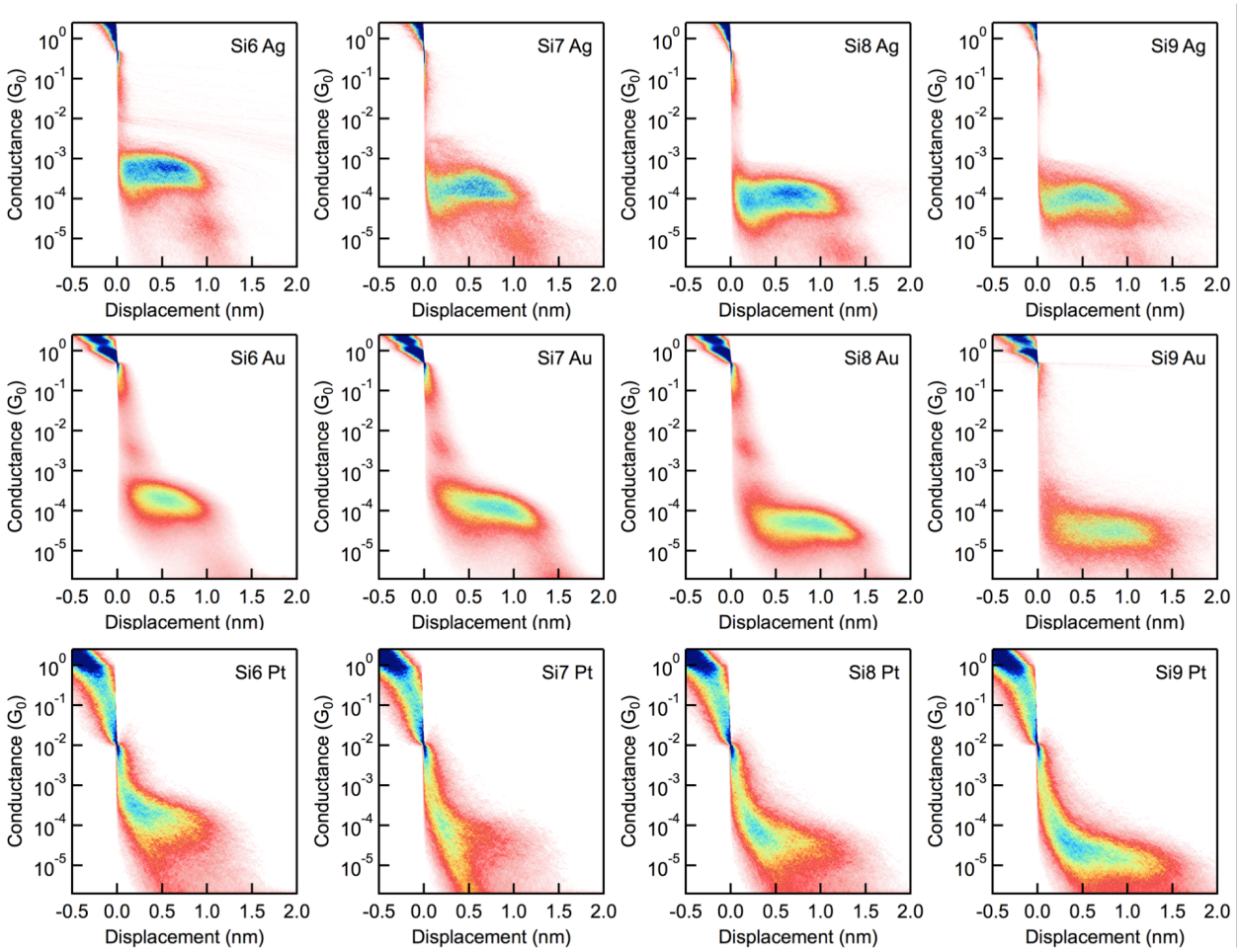

Figure S6. Two-dimensional (2D) conductance histograms for **Si6**-**Si9** measured with Au, Ag, and Pt electrical contacts.

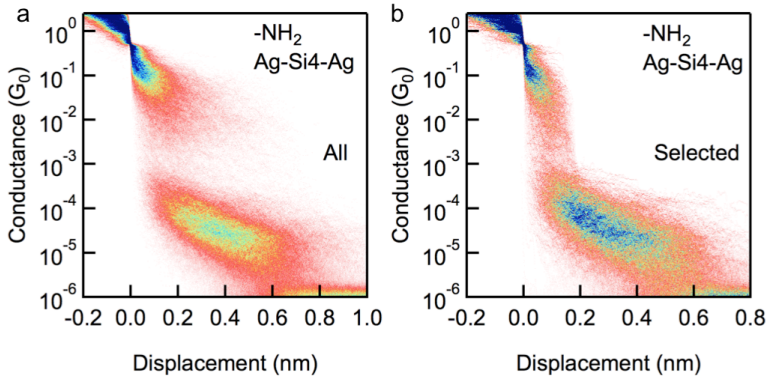

Figure S7. Two-dimensional (2D) conductance histograms constructed from (a) all traces and (b) selected traces of amine-terminated **Si4** measured with Ag electrical contacts. The same data were used for creating the 1D histograms in **Figure S3b**.

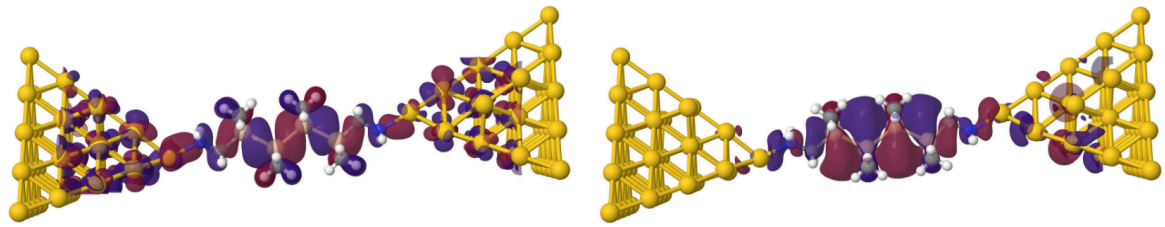

Figure S8. Isosurface plot of the scattering states at the HOMO and LUMO peaks for the Au-NH_2-**Si4**-NH_2-Au junction.

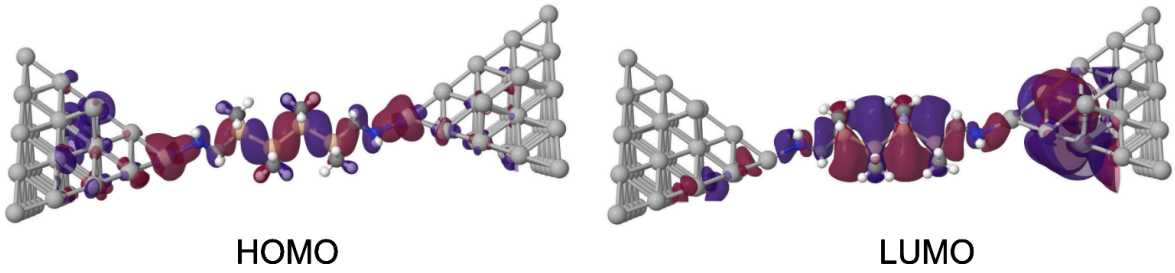

Figure S9. Isosurface plot of the scattering states at the HOMO and LUMO peaks of Ag-NH_2-**Si4**-NH_2-Ag junction.

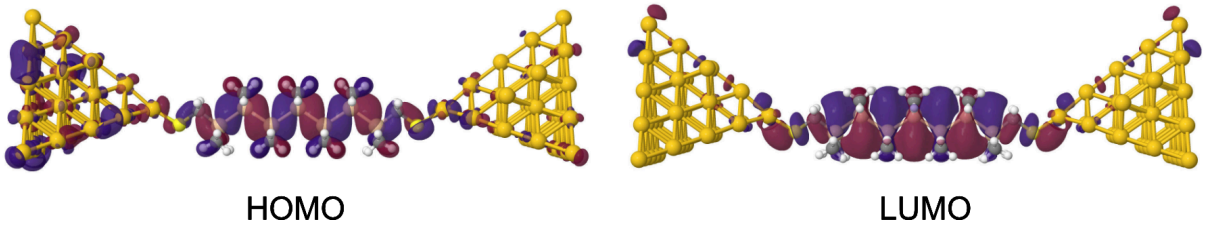

Figure S10. Isosurface plot of the scattering states at HOMO and LUMO peaks of Au-S-**Si7**-S-Au junction.

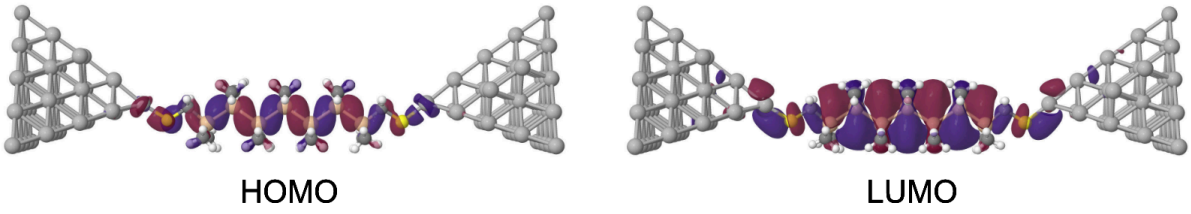

Figure S11. Isosurface plot of the scattering states at HOMO and LUMO peaks of Ag-S-**Si7**-S-Ag junction.

II. Synthetic Procedures and Characterization of Compounds

All reactions were performed in oven-dried or flame-dried round bottom flasks, unless otherwise noted. The flasks were fitted with rubber septa and reactions were conducted under a positive pressure of nitrogen or argon unless otherwise noted. Anhydrous and anaerobic solvents were obtained from a Schlenk manifold with purification columns packed with activated alumina and supported copper catalyst (Glass Contour, Irvine, CA). Automated flash chromatography was performed using a Teledyne Isco Combiflash R_f200 and Redisep R_f Gold Silica columns.

Materials. Commercial reagents were used without further purification unless otherwise noted. The syntheses of Cl-**Si**$_n$-Cl,[3] HS-CH_2-**Si**$_n$-CH_2-SH (n=2-4, 6),[4] MeS-CH_2-**Si**$_n$-CH_2-SMe,[3] and MeS-CH_2-**Ge**$_n$-CH_2-SMe[3] were previously reported.

Instrumentation. ^{1}H, ^{13}C, and ^{29}Si NMR spectra were recorded on a Bruker DRX300 (300 MHz), Bruker DRX400 (400 MHz) or a Bruker DMX500 (500 MHz) spectrometer. Chemical shifts for protons are reported in parts per million downfield from tetramethylsilane and are referenced to residual protium in the NMR solvent ($CHCl_3$: δ 7.26). Chemical shifts for carbon are reported in parts per million downfield from tetramethylsilane and are referenced to the carbon resonances of the solvent ($CDCl_3$ δ 77.16). Chemical shifts for silicon are reported in parts per million downfield from tetramethylsilane and referenced to the silicon resonance of tetramethylsilane (TMS δ 0.0). The silicon NMR resonances were determined with a DEPT pulse sequence. Data are represented as follows: chemical shift, multiplicity (s = singlet, d = doublet, dd= doublet of doublets, t = triplet, m = multiplet), coupling constants in Hertz, and integration. The mass spectroscopic data were obtained at the Columbia University mass spectrometry facility using a Waters XEVO G2XS QToF mass spectrometer equipped with a UPC2 SFC inlet, electrospray ionization (ESI) probe, atmospheric pressure chemical ionization (APCI) probe, and atmospheric solids analysis probe (ASAP+).

Synthetic Details

I. α,ω-bis(acetylthiomethyl)permethyloligosilanes (*n*=7-9) **Si*n*-CSAc**

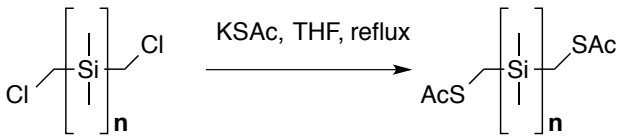

The thioacetate-terminated oligosilanes were synthesized from previously reported methods.[4] Potassium thioacetate (46 mg, 0.400 mmol, 2.40 equiv.) was added to a 10 mL round bottom flask equipped with a stir bar and condenser followed by 1.5 mL THF. 1,7-bis(chloromethyl) tetradecamethylheptasilane (84 mg, 0.167 mmol, 1.00 equiv.) was

dissolved in 1.5 mL THF and added to the flask at room temperature. The reaction mixture was refluxed overnight. The solvent was removed *in vacuo* and the crude material was passed through a silica plug with dichloromethane. The mixture was concentrated *in vacuo* to yield a crude orange oil. The crude material was purified by a automated silica gel chromatography with a gradient from hexanes to 7:3 hexanes:ethyl acetate. The product was isolated as an orange semi-solid (87 mg, 89% yield). ^{1}H NMR (400 MHz, $CDCl_3$) δ 2.33 (s, 6H), 2.20 (s, 4H), 0.21 (s, 6H), 0.21 (s, 12H), 0.19 (s, 12H), 0.15 (s, 12H). ^{13}C NMR (126 MHz, $CDCl_3$) δ 197.05, 30.33, 13.72, -2.94, -3.93, -4.12, -5.13. ^{29}Si NMR (60 MHz, $CDCl_3$) δ -12.68, -37.78, -39.22, -42.89. HRMS (TOF MS ASAP+) for $C_{20}H_{52}O_2S_2Si_7H$ ($[M+H]^+$): calculated = 585.1872, found = 585.1882.

n=8: The 1,8-bis(acetylthiomethyl)hexadecamethyloctasilane was synthesized with the same general procedure as above with the following exceptions: 1,8-bis(chloromethyl) hexadecamethyloctasilane was used instead of 1,7-bis(chloromethyl)tetradecamethylheptasilane. Orange semi-solid (78 mg, 70% yield). ^{1}H NMR (400 MHz, $CDCl_3$) δ 2.34 (s, 6H), 2.20 (s, 4H), 0.21 (s, 12H), 0.21 (s, 12H), 0.19 (s, 12H), 0.15 (s, 12H). ^{29}Si NMR (60 MHz, $CDCl_3$) δ -12.68, -37.69, -39.16, -42.88. HRMS (TOF MS ASAP+) for $C_{22}H_{58}O_2S_2Si_8H$ ($[M+H]^+$):: calculated = 643.2111, found = 643.2125.

n=9: The 1,9-bis(acetylthiomethyl)octadecamethylnonasilane was synthesized with the same general procedure as above with the following exceptions: 1,9-bis(chloromethyl) octadecamethylnonasilane was used instead of 1,7-bis(chloromethyl)tetradecamethylheptasilane and the crude material was carried forward without purification. Orange semi-solid (161 mg, 93% yield). ^{1}H NMR (500 MHz, $CDCl_3$) δ 2.34 (s, 6H), 2.20 (s, 4H), 0.21 (s, 12H), 0.21 (s, 6H), 0.20 (s, 12H), 0.19 (s, 12H), 0.15 (s, 12H). ^{13}C NMR (126 MHz, $CDCl_3$) δ 197.07, 30.34, 13.74, -2.94, -3.84, -3.86, -4.08, -5.11. ^{29}Si NMR (99 MHz, $CDCl_3$) δ -12.71, -37.64, -37.66, -39.19, -42.92. HRMS (TOF MS ASAP+) for $C_{24}H_{64}O_2S_2Si_9H$ ($[M+H]^+$):: calculated = 701.2349, found = 701.2352.

II. α,ω-bis(methylthiol)permethyloligosilanes (*n*=7-9) **Si*n*-CSH**

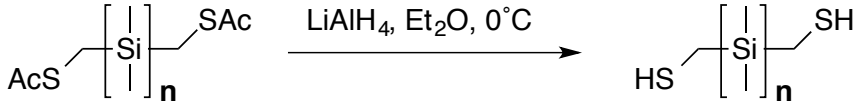

The thiol-terminated oligosilanes were synthesized from previously reported methods.[4] Lithium aluminum hydride (25 mg, 0.673 mmol, 5.06 equiv.) was added to an oven-dried 10 mL round bottom flask equipped with a stir bar and rubber septum. 2 mL Et_2O was added to the flask and the flask was cooled to 0˚C. 1,7-bis(acetylthiomethyl)tetradecamethylheptasilane (67 mg, 0.133 mmol, 1.00 equiv.) was

dissolved in 2 mL Et_2O and added dropwise. After stirring for one hour, the reaction mixture was quenched at 0˚C by dropwise addition of a 2 M HCl solution (0.35 mL), after which the reaction mixture was stirred at room temperature for 5 minutes. Sodium sulfate was added to the reaction mixture and stirred for 5 minutes. The reaction mixture was filtered over an alumina plug and the solids were rinsed with Et_2O as eluent. Solvent was removed *in vacuo* to yield a white semisolid (50 mg, 75% yield). ^{1}H NMR (400 MHz, $CDCl_3$) δ 1.78 (d, *J* = 6.9 Hz, 4H), 1.17 (t, *J* = 6.8 Hz, 2H), 0.22 (s, 6H), 0.21 (s, 12H), 0.20 (s, 12H), 0.18 (s, 12H). ^{13}C NMR (101 MHz, $CDCl_3$) δ 7.86, -3.58, -3.89, -4.08, -4.97. ^{29}Si NMR (60 MHz, $CDCl_3$) δ -10.48, -37.81, -39.20, -43.06. HRMS (TOF MS ASAP+) for $C_{16}H_{48}S_2Si_7$–2H+H (Ionizes as the disulfide [(M-2H) +H]$^+$): calculated = 499.1504, found = 499.1493.

n=8: The 1,8-bis(methylthiol)hexadecamethyloctasilane was synthesized with the same general procedure as above with the following exceptions: 1,8-bis(acetylthiomethyl) hexadecamethyloctasilane was used instead of 1,7-bis(acetylthiomethyl)tetradecamethyl-heptasilane. White semisolid (50 mg, 96% yield). ^{1}H NMR (400 MHz, $CDCl_3$) δ 1.78 (d, *J* = 6.9 Hz, 4H), 1.17 (t, *J* = 6.9 Hz, 2H), 0.21 (s, 12H), 0.21 (s, 12H), 0.20 (s, 12H), 0.18 (s, 12H). ^{13}C NMR (101 MHz, $CDCl_3$) δ 7.88, -3.57, -3.85, -4.05, -4.95. ^{29}Si NMR (60 MHz, $CDCl_3$) δ -8.74, -27.11, -28.29, -32.60. HRMS (TOF MS ASAP+) for $C_{18}H_{54}S_2Si_8$–2H+H (Ionizes as the disulfide [(M-2H) +H]$^+$): calculated = 557.1743, found = 557.1753.

n=9: The 1,9-bis(methylthiol)octadecamethylnonasilane was synthesized with the same general procedure as above with the following exceptions: 1,9-bis(acetylthiomethyl) octadecamethylnonasilane was used instead of 1,7-bis(acetylthiomethyl)tetradecamethyl-heptasilane and the crude material was purified by an Al_2O_3 chromatography with 100% hexanes as eluent. White semisolid (58 mg, 41% yield). ^{1}H NMR (400 MHz, $CDCl_3$) δ 1.78 (d, *J* = 6.9 Hz, 4H), 1.17 (t, *J* = 6.9 Hz, 2H), 0.21 (s, 12H), 0.21 (s, 12H), 0.21 (s, 6H), 0.20 (s, 12H), 0.19 (s, 12H). ^{13}C NMR (126 MHz, $CDCl_3$) δ 7.87, 0.16, -3.58, -3.82, -3.84, -4.05, -4.96. ^{29}Si NMR (99 MHz, $CDCl_3$) δ -10.49, -37.63, -37.67, -39.16, -43.07. (TOF MS ASAP+) for $C_{20}H_{60}S_2Si_9$–2H+H (Ionizes as the disulfide [(M-2H) +H]$^+$): calculated = 615.1982, found = 615.1998.

Si4-CNPhth

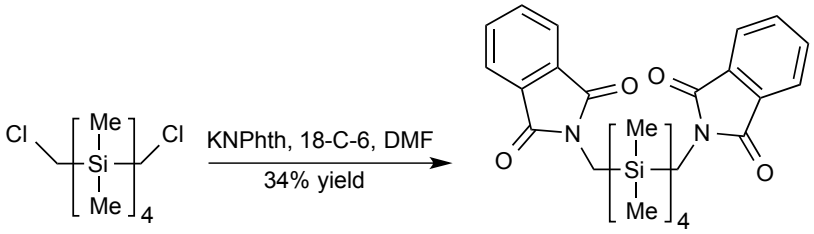

A 20 mL scintillation vial equipped with a stir bar was charged with potassium phthalimide (359 mg, 1.94 mmol, 2.02 equiv.) and 18-crown-6 (23 mg, 0.086 mmol, 0.09 equiv.). 2 mL dimethylformamide (DMF) was added to the vial, followed by 1,4-bis(chloromethyl)octamethyl-tetrasilane (319 mg, 0.96 mmol, 1.00 equiv.) dissolved in 1 mL DMF. The suspension was stirred at room temperature overnight. The solvent was removed *in vacuo* and the crude material was dissolved in ether, washed 3x with distilled water, washed 1x with brine, dried over sodium sulfate, then filtered. After removing the solvent *in vacuo*, the crude material was chromatographed with a gradient of hexanes to 4:1 hexanes:ethyl acetate to yield Si4-CNPhth as a white solid (178 mg, 34% yield). ^{1}H NMR (500 MHz, $CDCl_3$) δ 7.80 (dd, *J* = 5.4, 3.1 Hz, 4H), 7.67 (dd, *J* = 5.5, 3.0 Hz, 4H), 3.32 (s, 4H), 0.23 (s, 12H), 0.18 (s, 12H). ^{13}C NMR (126 MHz, $CDCl_3$) δ 168.57, 133.76, 132.46, 123.04, 28.28, -2.86, -5.56. ^{29}Si NMR (99 MHz, $CDCl_3$) δ -11.38, -44.50. (TOF MS ASAP+) for $C_{26}H_{36}N_2O_4Si_4$+H ($[M+H]^+$): calculated = 553.1830, found = 553.1827.

Si4-CNH_2

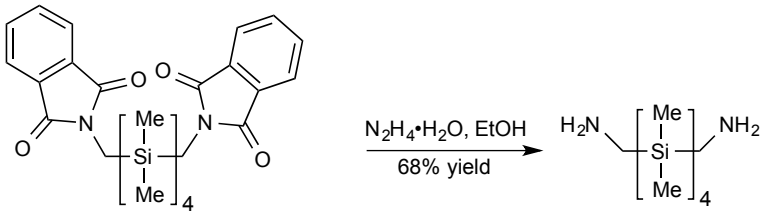

A 10 mL Schlenk flask equipped with a rubber septum and stir bar was charged with Si4-CH_2Phth (72 mg, 0.131 mmol, 1.00 equiv.). Ethanol (2 mL) was added to the flask, followed by hydrazine monohydrate (0.06 mL, 1.16 mmol, 8.87 equiv.). The flask was equipped with a reflux condenser and was stirred at 75˚C in an oil bath overnight. The reaction mixture was cooled to room temperature, then filtered over Celite with THF as eluent. The mixture was concentrated *in vacuo*. Water was added, and the aqueous layer was extracted with dichloromethane (3 x 10 mL). The combined organic layer was dried over sodium sulfate, filtered, and concentrated to yield Si4-$CHNH_2$ as a pale yellow oil (26 mg, 68% yield). ^{1}H NMR (500 MHz, $CDCl_3$) δ 2.32 (s, 4H), 1.30 (broad s, 4 H), 0.16 (s, 12H), 0.13 (s, 12H). ^{13}C NMR (126 MHz, $CDCl_3$) δ 77.16, 30.92, -4.54, -5.41. ^{29}Si NMR (99 MHz, $CDCl_3$) δ -13.19, -44.98. (ESI+) for $C_{10}H_{32}N_2Si_4$+H ($[M+H]^+$): calculated = 293.1721, found = 293.1721.

III. STM Break Junction Experiment Details

We measured the conductance of single molecules bound to Au, Ag and Pt electrodes using a home-built modified Scanning Tunneling Microscope (STM). A commercially available single-axis piezoelectric positioner (Nano-P15, Mad City Labs) was used to achieve sub-angstrom level control of the tip-substrate distance. The STM was controlled using a custom written program in IgorPro (Wavemetrics, Inc.) and operated in ambient conditions at room temperature, except for Pt measurements we flush the setup chamber with argon. The gold substrate was cleaned using UV/Ozone for 15 minutes prior to use. The silver slug was mechanically polished prior to use. We use mechanically polished Ag and Pt slug (Alfa-Aesar, Ag: 99.99% purity, Pt: 99.9% purity) and Au-coated mica surface as the substrate, and the corresponding freshly cut 0.25mm diameter metal wire as the tip (Alfa-Aesar, Ag: 99.9985 % purity, Pt: 99.95% purity, Au: 99.998% purity). Prior to adding the solution of molecules, we collect 1000 traces to make sure the metal is clean in the measurement with Au and Ag metal contacts. The platinum slug was mechanically polished, then immediately rinsed and sonicated in acetone prior to the measurement of molecules. Solutions of the target molecules at 1 mM concentration in 1,2,4-trichlorobenzene (Alfa Aesar, 99% purity) were added to the substrate for molecular conductance measurements. The applied bias was 225 or 900 mV, and the substrate was displaced at a speed of 19 nm/s or 38 nm/s for all measurements. The current and voltage data were acquired at 40 kHz.

Junction elongation length

From each molecule we determine a junction elongation length distribution by integrating the 2D histogram over half a decade in conductance centered at the molecular conductance peak. To define the distance that a single molecule junction can be elongated before its final rupture, we determine the distance at which the counts drops to 5% of its peak value for each molecule measured and plot this in Figure 2c in the manuscript as a function of the number of silicon atoms in the backbone.

IV. Theoretical Calculations Details

Our *ab-initio* quantum transport calculations are based on a finite cluster approach. Kohn-Sham states are represented in an optimized all-electron localized basis set (tier1 – 'light' settings, similar to 'double-zeta' quality) with convergence criteria for the difference in the ground state density (10^{-5}), total energy (10^{-6} eV) and forces (10^{-4} eV/Å). The procedure to obtain the geometries for the transport calculations proceeds in two steps. First, the positions of the molecular atoms and the apex of the electrodes are optimized. The clusters used for this geometry optimization contain up to 11 Au (Ag)

atoms per pyramid and structural relaxation is performed using an enhanced version of the Broyden-Fletcher-Shanno-Goldfarb algorithm[5] until all the components of the residual forces per atom fall below 10^{-2} eV/Å. In a second step, the geometry is fixed and new layers of Au (Ag) are added to the outer planes of both pyramids to ensure the proper screening of the excess charge in the subsequent transport calculations.

Note that, while our DFT-based transport calculations reproduce experimental trends reliably on a qualitative level, the relative order of conductance in the case of thiols is not predicted: the reversal of conductance seen in the experiments between amine and thiol linkers is not fully seen in our calculations. We attribute this discrepancy to the imperfect description of the relative alignment of energy levels (> 0.1 eV) within Kohn-Sham transport calculations. In particular, in the present calculation one cannot rely upon cancellations of errors of exchange-correlation functionals, because relativistic corrections and spin-orbit interaction shifts contribute more significantly to Au junctions than for Ag.[6]

Scalar-relativistic calculations

Incorporation of relativistic effects in *ab-initio* calculations becomes increasingly important as we go down the periodic table of elements. The zeroth order regular approximation (ZORA) implemented in FHI-aims has been designed to provide an efficient relativistic description of the valence and outer core electrons. For deep core levels of heavy atoms, however, ZORA can lead to inaccuracies.[7] To check the impact on our calculations, we compare all electron calculations on the ZORA level with an alternative method to incorporate relativistic corrections relying on effective core potentials (ECP). We recall that ECPs can be constructed by fitting to all-electron, fully relativistic calculations.[8-9]

Specifically, we verify that differences in the relativistic treatment do not lead to systematic errors in the transmission curves that could affect our interpretation. To this end, we compare two structures: the **Si7** with thiol linkers bound to Ag and Au leads. The ECP calculation was performed with Turbomole 7.1, PBE functional and without additional relaxation of the geometry. The def2-TZVP (triple-zeta) basis set was employed and the calculation was converged with respect to the spherical grid size. The calculation of the transmission function was done with an embedding self-energy identical to the one used for the FHI-AIMS calculation.

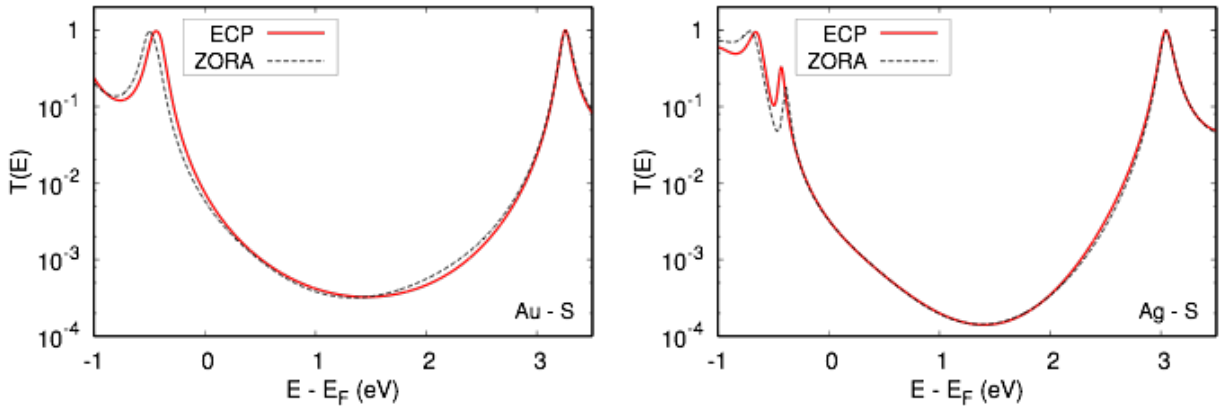

Figure S12. Transmissions for the Au-S junction (left) and the Ag-S junction (right). Each plot compares the two approximate relativistic treatments, ECP and ZORA, described in the accompanying text.

The transmission functions are compared in Figure S11. They are altogether very similar. The HOMO resonances are shifted up in ECP against ZORA by approximately 80 meV. Because of the shift, the conductance of Au—S junction differs by 25% between ZORA and ECP. In Ag—S junction, the gateway state gains considerably more weight in the ECP calculation. The difference in conductance between ZORA and ECP is 2%, which is comparable to the error due to basis sets, and is therefore insignificant. This reflects the fact that the density of states in Ag at the Fermi level is dominated by sp electrons, whose relativistic effects are negligible. The order of the transmissions (Ag—S vs Au—S) remains the same in ZORA and ECP, confirming the interpretation of the Kohn-Sham transport calculations in the main text.

V. NMR spectra

Si7-CSAc

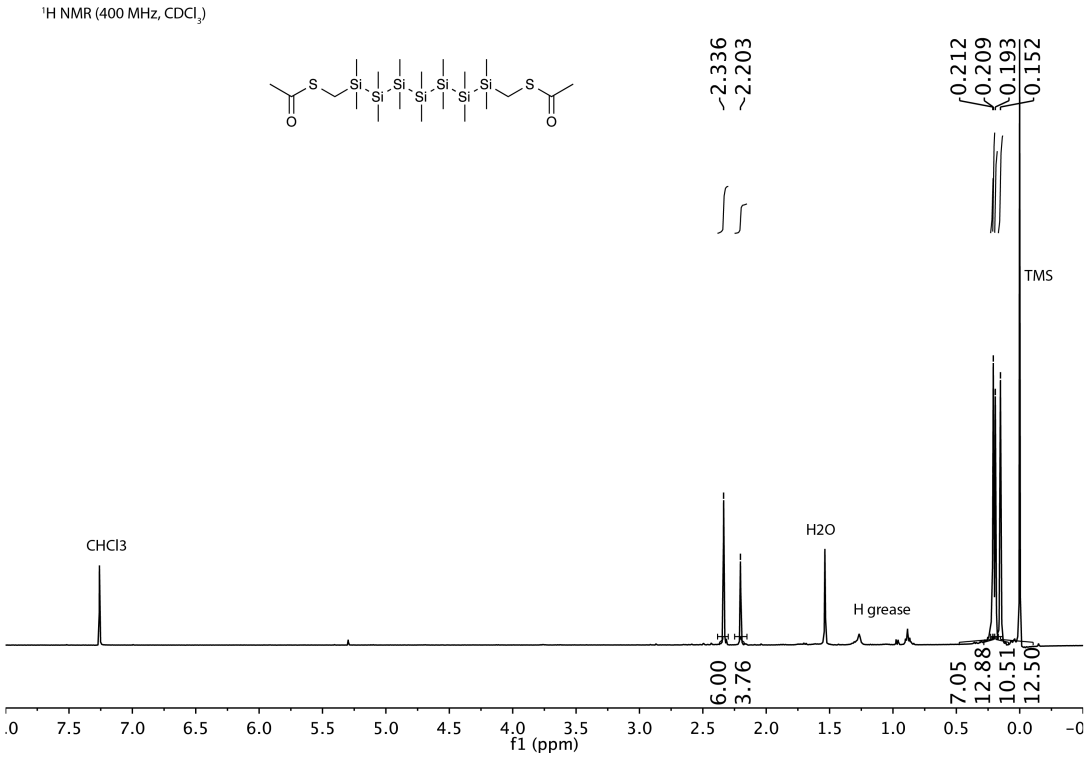

Si8-CSAc

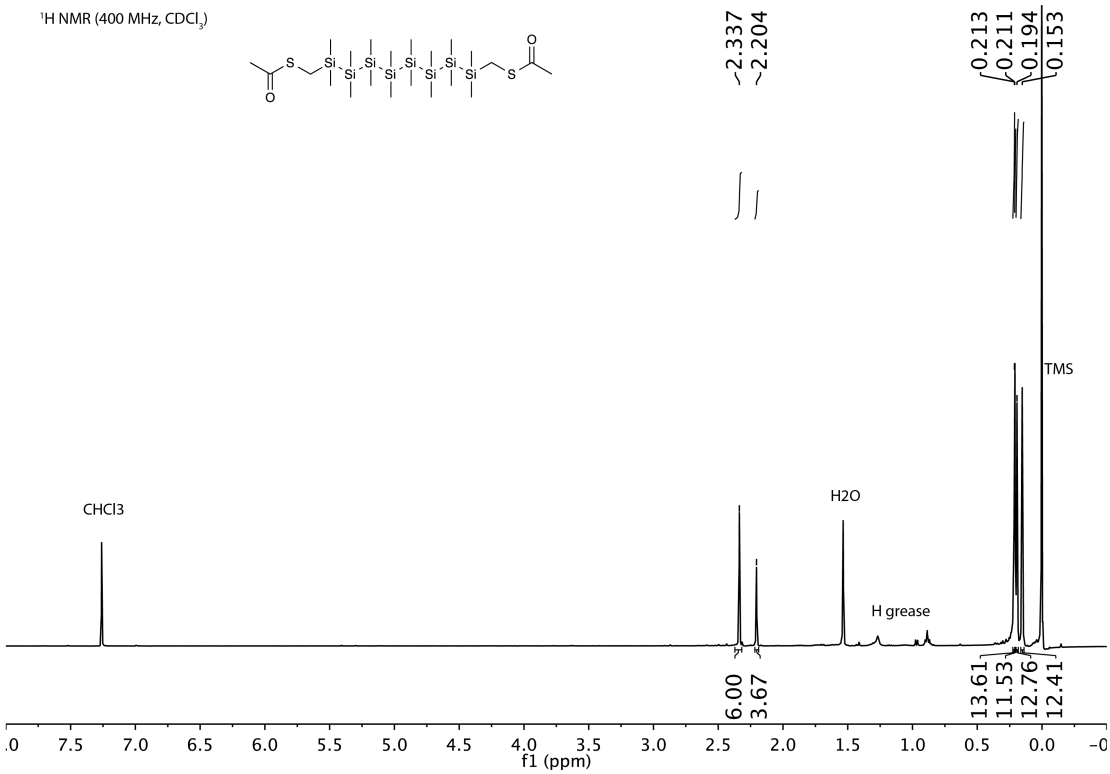

Si9-CSAc

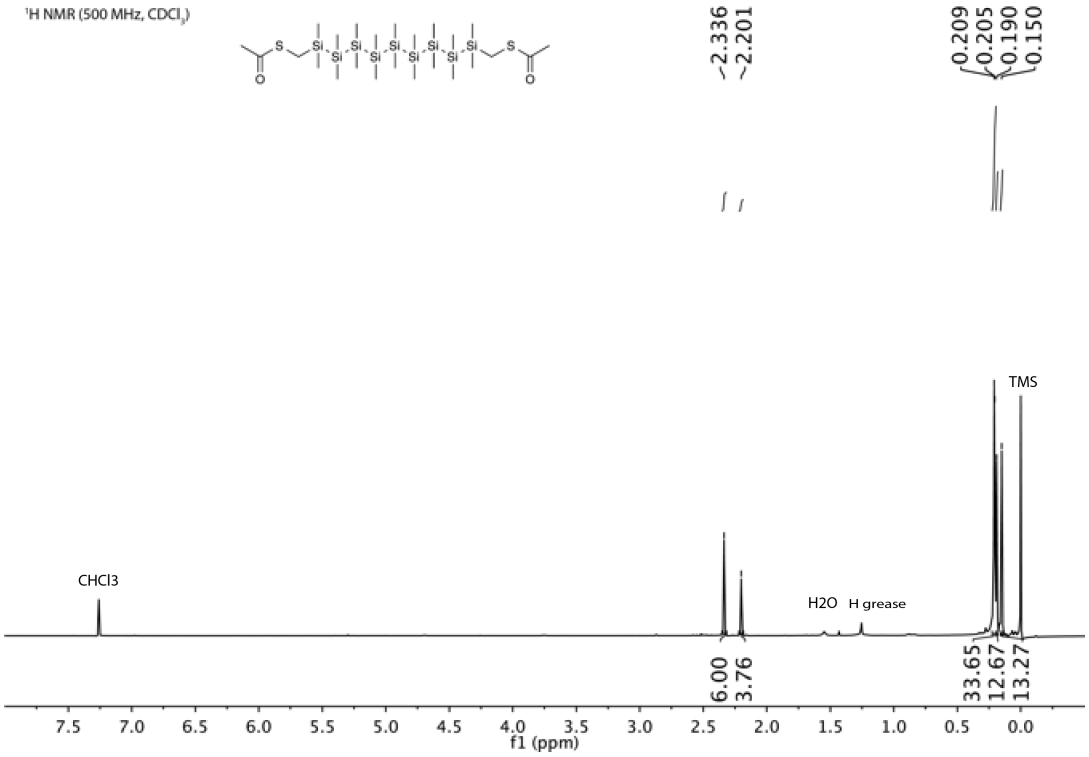

Si7-CSH

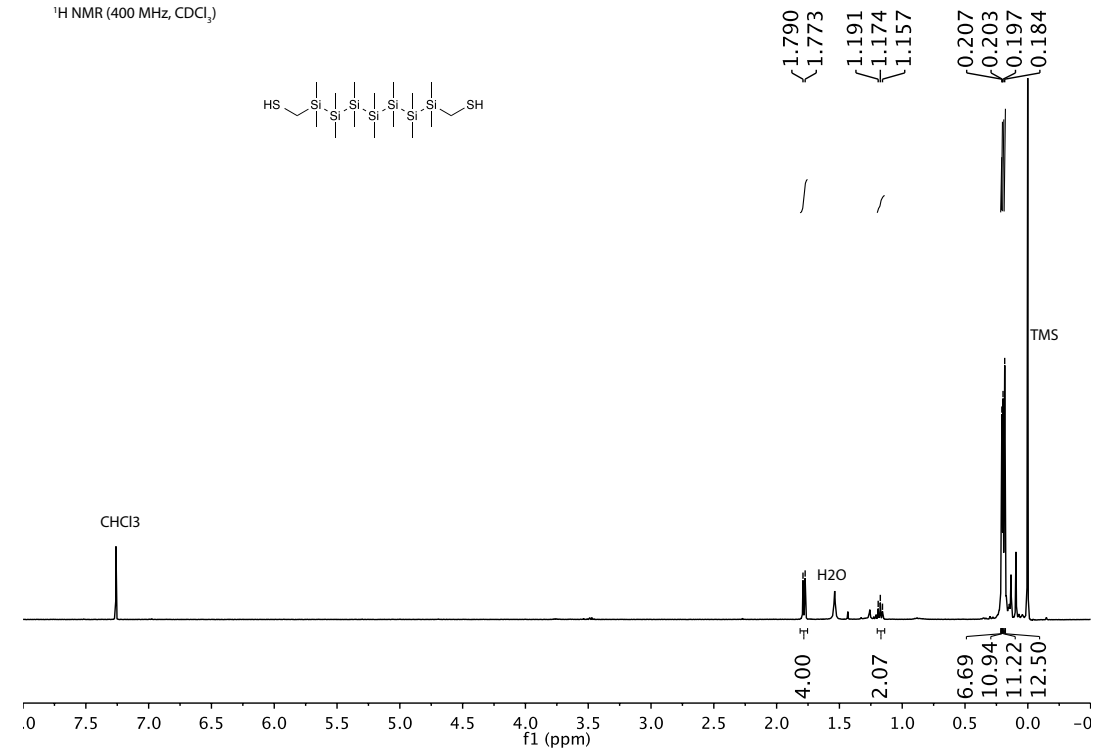

Si8-CSH

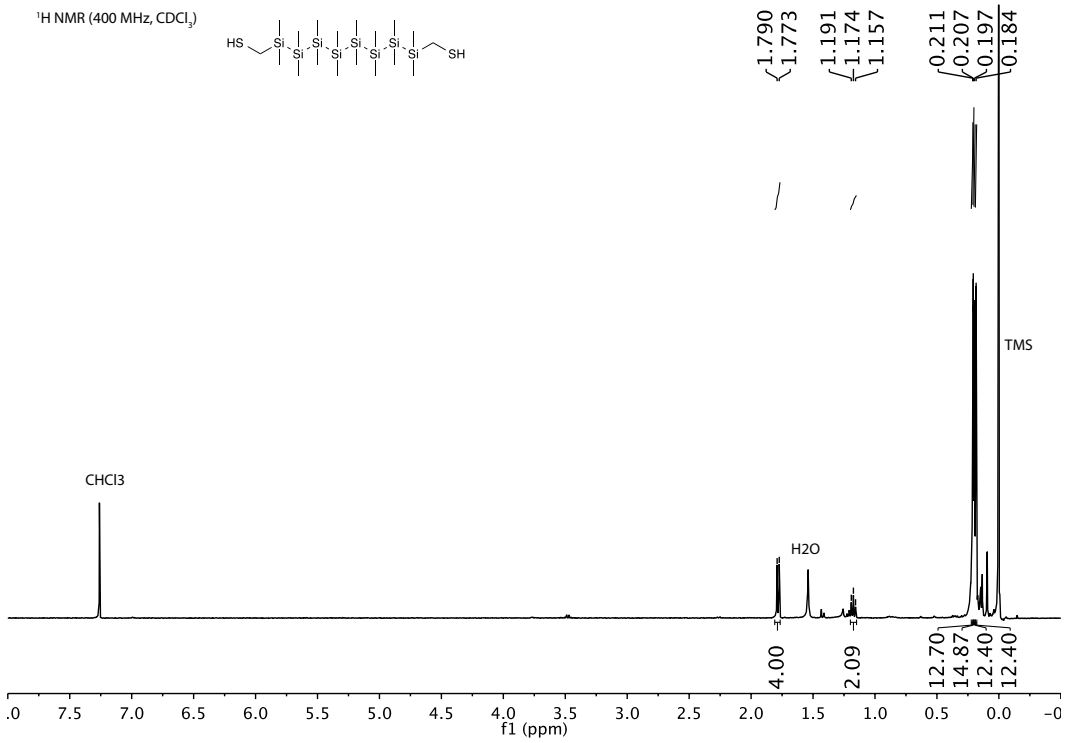

Si9-CSH

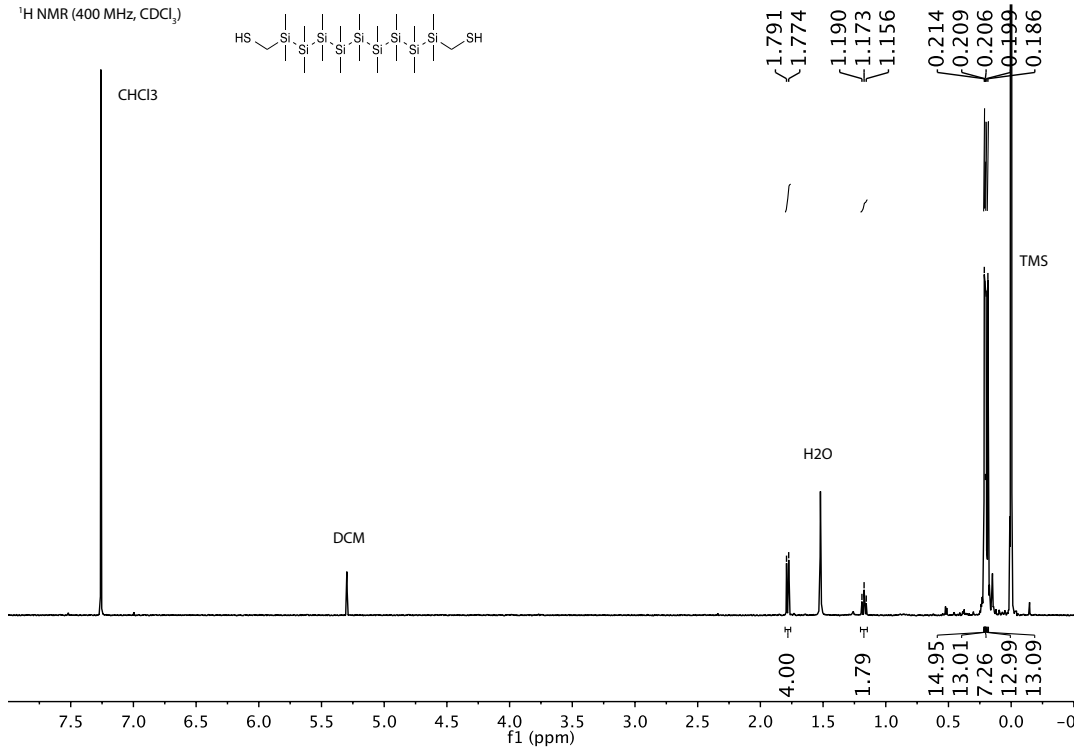

Si4-CNH$_2$

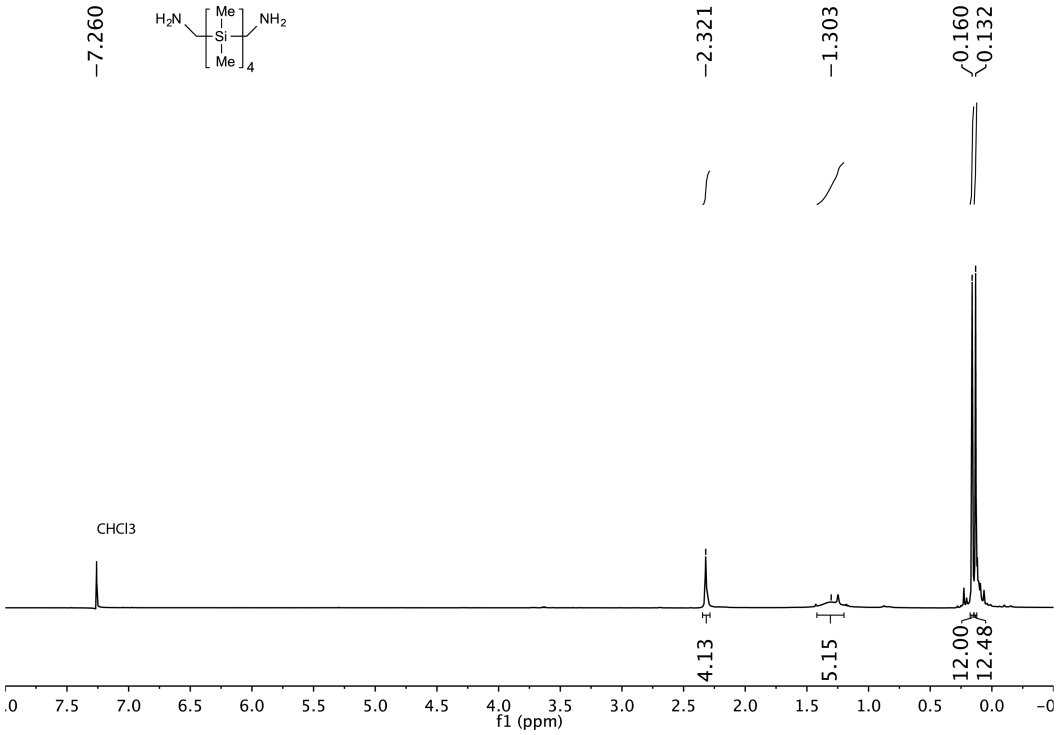

Si4-CNPhth

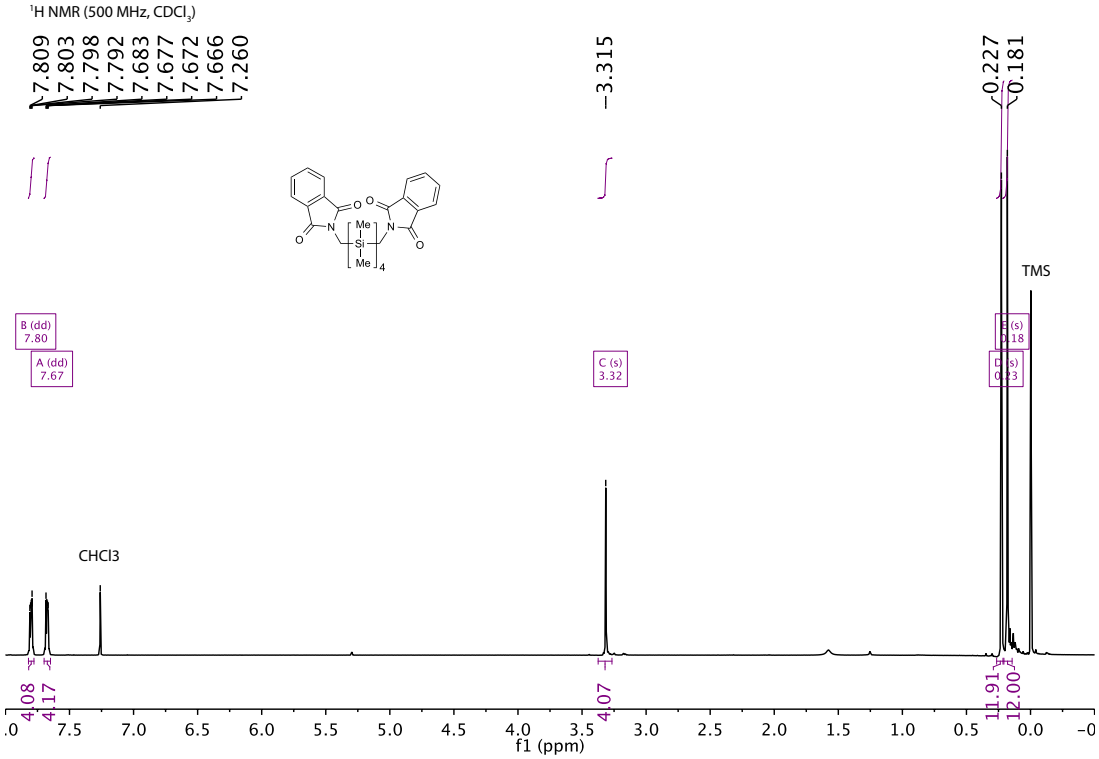

V. References

1. Inkpen, M. S.; Leroux, Y. R.; Hapiot, P.; Campos, L. M.; Venkataraman, L., Reversible on-surface wiring of resistive circuits. *Chem. Sci.* **2017,** *8* (6), 4340-4346.

2. Kim, T.; Vázquez, H.; Hybertsen, M. S.; Venkataraman, L., Conductance of Molecular Junctions Formed with Silver Electrodes. *Nano Lett.* **2013,** *13* (7), 3358-3364.

3. Su, T. A.; Li, H.; Steigerwald, M. L.; Venkataraman, L.; Nuckolls, C., Stereoelectronic switching in single-molecule junctions. *Nat. Chem.* **2015,** *7* (3), 215-220.

4. Li, H.; Su, T. A.; Zhang, V.; Steigerwald, M. L.; Nuckolls, C.; Venkataraman, L., Electric Field Breakdown in Single Molecule Junctions. *J. Am. Chem. Soc.* **2015,** *137* (15), 5028-5033.

5. Blum, V.; Gehrke, R.; Hanke, F.; Havu, P.; Havu, V.; Ren, X.; Reuter, K.; Scheffler, M., Ab initio molecular simulations with numeric atom-centered orbitals. *Comput. Phys. Commun.* **2009,** *180* (11), 2175-2196.

6. Li, C.; Pobelov, I.; Wandlowski, T.; Bagrets, A.; Arnold, A.; Evers, F., Charge Transport in Single Au | Alkanedithiol | Au Junctions: Coordination Geometries and Conformational Degrees of Freedom. *J. Am. Chem. Soc.* **2008,** *130* (1), 318-326.

7. Huhn, W. P.; Blum, V., One-hundred-three compound band-structure benchmark of post-self-consistent spin-orbit coupling treatments in density functional theory. *Physical Review Materials* **2017,** *1* (3), 033803.

8. Bergner, A.; Dolg, M.; Küchle, W.; Stoll, H.; Preuß, H., Ab initio energy-adjusted pseudopotentials for elements of groups 13–17. *Molecular Physics* **1993,** *80* (6), 1431-1441.

9. Arnold, A.; Weigend, F.; Evers, F., Quantum chemistry calculations for molecules coupled to reservoirs: Formalism, implementation, and application to benzenedithiol. *J. Chem. Phys.* **2007,** *126* (17), 174101.